CHAPTER 5

Roles of Re-entrant Cluster glass state and Spin lattice coupling in magneto-dielectric behavior of giant dielectric double perovskite $La_{1.8}Pr_{0.2}CoFeO_6$

5.1 Introduction:

The strong coupling between magnetic and electrical ordering is one of the key issues to realize the multifunctional materials for potential applications [248-251]. In this regard, double perovskites (DP) $A_2BB'O_6$ (where A is rare earth or alkaline ions, B/B' are transition metal ions) with rock salt ordered structure [252] are forming the promising classes of multifunctional materials which exhibit unique physical properties such as near room temperature ferromagnetic insulating ground state, large magneto-dielectric effect (MDE), Griffiths phase, giant exchange bias, low temperature re-entrant glassy states, spin-phonon coupling etc [18, 21, 21, 68, 70, 71]. Recently, A_2CoFeO_6 types of DP oxides have gained attention due to their high temperature phase transitions [17]. In fact, Co and Fe ions have their own features as they have similar size and valance states. So far, very limited number of studies have been reported on the DP oxides with Co-Fe combination for different rare earth ions and alkaline ions (A = Pr, La, Ho, Sr). Moreover, among multifunctional material properties, magneto-dielectric effect (MDE) is one of the most fascinating and auspicious characteristics in both scientific and technological aspects [253, 254]. Therefore, Co-Fe combined DP systems have wide scope to explore the magneto-dielectric effects. In fact, La based DP systems show large MDE close to room temperature [20,255-256]. So far, there is no report on the magneto-dielectric effect of La based Co-Fe combined DP system. Therefore, we were interested to investigate the La based Co-Fe combined DP, but could not succeed to synthesize the same. However, we successfully prepared the $La_{1.8}Pr_{0.2}CoFeO_6$ (LPCFO) *i.e.* by doping Pr on La site.

In the present chapter, we have investigated the effect of Pr^{3+} ion on La_2CoFeO_6 (LCFO) DP. As, one of the parent DP LCFO undergo a long range antiferromagnetic transition (~270

K) [68]. Whereas, the another parent Pr_2CoFeO_6 (PCFO) DP exhibits different magnetic states like Griffith phase, reentrant cluster glass, exchange Bias effect, spin phonon coupling and G type long range canted antiferromagnetic ordering at T_N = 269 K [70, 71]. In the present paper, we have shown along with antiferromagnetic (AFM) ordering, $La_{1.8}Pr_{0.2}CoFeO_6$ (LPCFO) exhibits a reentrant cluster glass transition at low temperature as well as large dielectric constant with low loss. Interestingly, negative magneto dielectric has also been observed both at low and high temperatures. A correlation between the spin freezing and spin-lattice coupling with observed MDE has been established for this compound.

5.2 Experiment:

Pure oxides of La_2O_3, Pr_6O_{11}, CoO and Fe_2O_3 powders were taken in a stoichiometric ratio as precursors and ground them. The ground powder was calcined at 1000^oC for 24 hours in air. Again same calcined process was carried out at several times at 1200^oC for 24 hours. At last, the pressed pellets were sintered at 1350^oC for 36 hours followed by slow cooling rate (30^oC/hour). The phase purity of sample were studied by X- ray diffractometer (model: Miniflex II, Rigaku, Japan) with Cu Kα radiation (λ=1.5406 Å) operating at 40 kV and 30 mA. The temperature dependent DC and AC magnetic measurements were carried out using superconducting quantum interference device (SQUID) based magnetic property measurement system (MPMS). The X- ray absorption spectroscopy (XAS) data of this sample was recorded at the BL-14 beamline of Hiroshima Synchrotron Radiation Centre, Hiroshima University, Japan. The transport properties were measured by Keysight E4980A

Precision LCR meter. Raman spectra were taken by Renishaw Micro Raman Spectrometer using a solid state Laser of wavelength 532 nm.

5.3 Results:

5.3.1 Stability and Structure Study:

The stability of a crystal can be determined by tolerance factor (*t*), for mixed A-site $A_{2-x}A'_xBB'O_6$ double perovskites which can be determined by the equation [257]

$$t = \frac{\left(1-\frac{x}{2}\right)r_A+\left(\frac{x}{2}\right)r_{A'}+r_O}{\sqrt{2}\left(\frac{r_B}{2}+\frac{r_{B'}}{2}+r_O\right)} \quad (5.1)$$

where, r_A, $r_{A'}$, r_B, $r_{B'}$ and r_O are shannon ionic radius of respective ions. The calculated value of *t* for the present LPCFO sample is 0.85, suggesting the monoclinic/orthorhombic structure. Fig. 5.1 shows the Rietveld refinement of the x-ray diffraction (XRD) pattern of LPCFO compound at room temperature. LPCFO is crystallized into $P2_1/n$ (14) space group (in consistent with the *t*) unlike the end members LCFO with R-3c space group [68, 258] and PCFO with Pnma space group [70]. It is well known that orthorhombic structure has random distribution of B-site over the octahedral sites, whereas, monoclinic structure has ordered stacking of B-site ions. Therefore, LPCFO has an ordered structure in comparison to its both end members (LCFO and PCFO). The obtained lattice parameters of LPCFO from rietveld refinement are a = 5.484 Å, b = 5.447 Å, c = 7.715 Å and angle β is 89.997°.

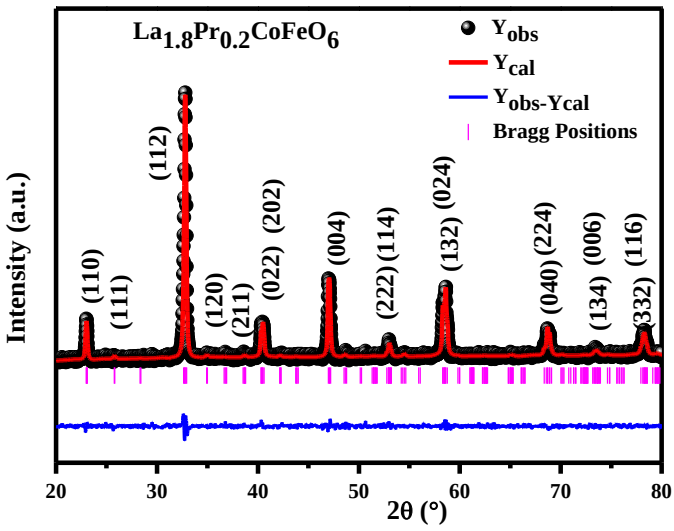

Figure 5.1: The XRD pattern along with the Rietveld refinement of LPCFO at 300 K.

5.3.2 XAS Study:

Figures 5.2a and 5.2b present the XAS spectra of Co ($L_{3,2}$) and Fe ($L_{3,2}$ edges) ions of LPCFO. The $L_{3,2}$ edge spectra of transition metal ions (B/B') are governed by the dipole transition from the 2p core level to unoccupied 3d (from $2p^6 3d^n$ to $2p^5 3d^{n+1}$) level. For Co2p XAS spectra (fig. 5.2a), the L_3 and L_2 peaks are at ~781.15 eV and ~795.68 eV respectively with a separation of ΔE ~14.5 eV which is associated to the spin-orbit coupling. No peak due to Co^{2+} around 777 eV is observed suggesting the presence of only trivalent Co ions in LPCFO. Further, the existence of narrow and sharp L_2 peak in LPCFO Co2p spectrum establishes the presence of Co^{3+} ions in low spin state (LS) at 300 K. The direct involvement of valance shells in $L_{3,2}$ edges of Co ions lead the XAS spectra highly sensitive to Co spin state. The similar characteristic features of Co^{3+} ions with LS have also been found in $LaCoO_3$ at 20 K [259] and in PCFO at 300 K [70]. The Fe2p XAS spectra of LPCFO (Fig. 5.2b) is divided into $FeL_3(2P_{3/2})$ and $FeL_2(2P_{1/2})$ peaks. The position of L_3 and L_2 peaks are at

~ 710.69 eV and ~723.18 eV respectively with a separation of ΔE ~13.3 eV. The L_3 and L_2 peaks are further split into t_{2g} and e_g doublet due to crystal field. The t_{2g} peaks are found 1.6 eV below the L_3 and L_2 peaks. The trivalent nature of Fe ions in LPCFO can be confirmed from the fact that its Fe2p XAS spectrum resembles with that of highly studied Fe_2O_3 system [260, 261] in which Fe ions are in +3 state.

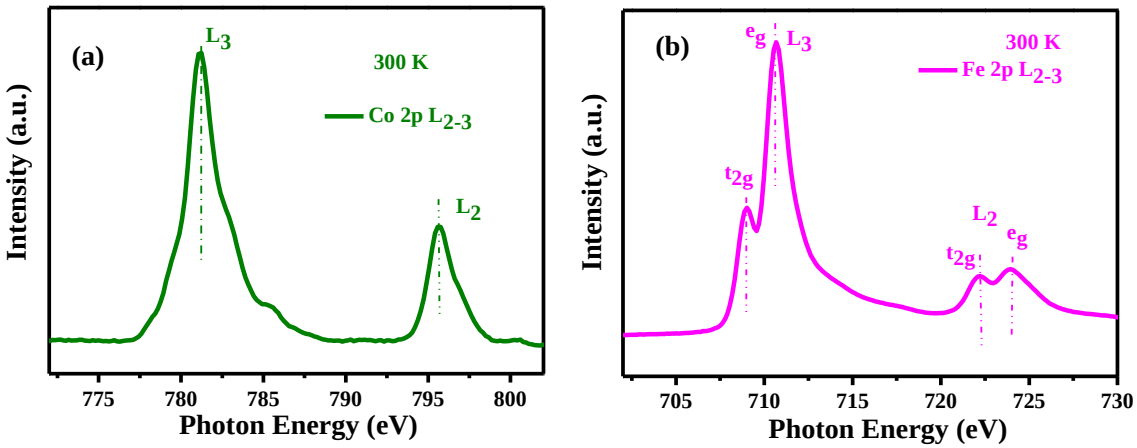

Figure 5.2: XAS spectra of **(a)** Co edge **(b)** Fe edge recorded at 300K.

5.3.3 Magnetic Study:

Figure 5.3a shows the temperature dependent DC magnetization of LPCFO sample at zero field cooled (ZFC) and field cooled (FC) protocols for different applied DC magnetic fields. Presence of large bifurcation between ZFC and FC curves indicates the existence of spin frustration. However, due to measurement limitation, we could not observe magnetic transition (T_N) at high temperature (>365K). Moreover, no inflection point has been identified in (dM/dT) curve (inset of fig. 5.3b) at high temperature (up to 365 K) but, an anomaly is observed at lower temperature side (T^*) in dM/dT curve, which suggests the

existence of another magnetic phase (reentrant) transition in LPCFO. A sharp transition around 100 K in ZFC curve is observed, similar to previously studied $LaCoO_3$ perovskite. Such anomaly has been considered as a thermally excited spin state transition from a low to an intermediate spin state of Co^{3+} ion [262, 263]. In present sample, Co^{3+} ion possesses a low spin state at 300 K. Therefore, it is quite possible that there is a spin state transition of Co^{3+} ions from a low to an intermediate spin state. However, the abrupt change in profound competition between the crystal field splitting (ΔC_F) energies and intra-atomic Hund's coupling (H_{ex}) due to applied higher magnetic field may be the reason of disappearance of this ~ 100 K transition.

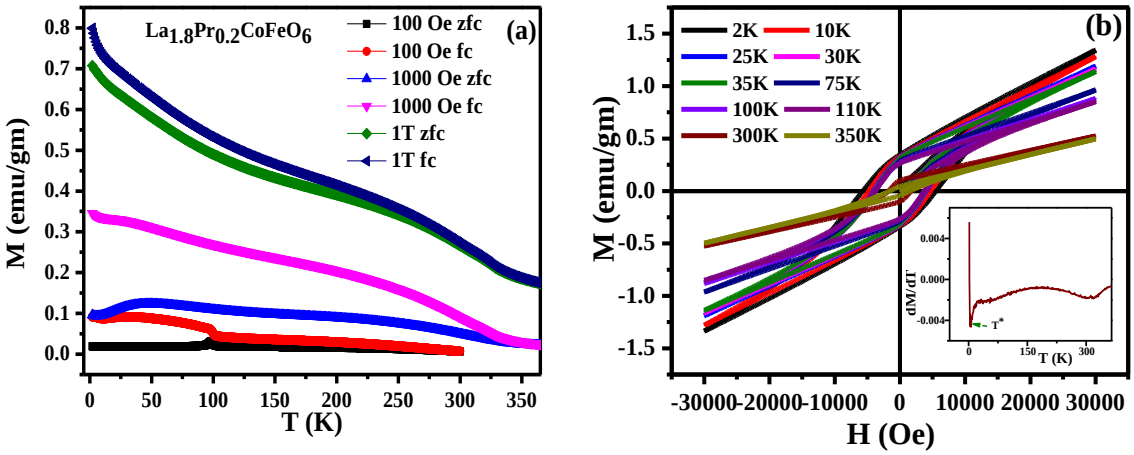

Figure 5.3: (a) The temperature dependent ZFC and FC Curve of LPCFO at different magnetic fields. **(b**) The isothermal (M-H) curves of LPCFO at different temperatures**. Inset**: dM/dT as a function of temperature.

Figure 5.3b shows the M(H) curve of LPCFO at different temperatures. It is obvious that even up to 350 K, system exhibits magnetic ordering as the observed unsaturated magnetic moment with small hysteresis loop confirming the presence of weak ferromagnetism. An increase in coercivity and magnetic moment with decrease in temperature can be seen from this figure. Unsaturated magnetic moment (presence of antiferromagnetic nature) can be attributed to the antiparallel alignment of Fe^{3+} spins, which arises due to Fe^{3+}/ Fe^{3+}

antiferromagnetic (AFM) interactions. Whereas, the canting of Fe^{3+} spins is the origin of small hysteresis loop which suggests the existence of weak ferromagnetism (FM) in LPCFO. The canting of Fe^{3+} spins (weak FM) is an inherent property of AFM orthoferrite systems, which can be understood by the Dzyaloshinskii-Moriya (DM) interaction [142, 264]. Therefore, above discussion suggests that LPCFO possesses predominant canted antiferromagnetic spin ordering.

As we mentioned above, there is another magnetic phase transition (T^* in dM/dT curve) present at low temperature. This low temperature transition is an indication of glassy magnetic phase transition, as sudden bifurcation is observed in DC ZFC and FC curves. Therefore, to examine the low temperature magnetic phase transition, the AC susceptibility measurement in 2-100 K temperature range was performed. Figures 5.4a and 5.4b show the temperature dependent real $\chi'(T)$ and imaginary $\chi''(\mathrm{T})$ part of AC susceptibility of LPCFO at zero field, respectively. The $\chi'(T)$ show a drop below 50 K, corresponding clear peak in $\chi''(\mathrm{T})$ is observed at T~ 31 K. The positions of these peaks are shifted towards higher temperature side with increasing frequencies. This key feature predicts the spin glass (SG) or cluster glass (CG) transition at low temperature [20, 265-268]. The explanation for the existence of glassy nature in present sample can be manifested by the anti-site disorder and spin canting [20, 266] which are present in LPCFO system. The first one, the B- site disorder i.e., random site distribution of B- site ions drives the Fe^{3+} and Co^{3+} to be randomly distributed causing the spin frustration in the system. The second one, i.e., spin canting, is induced in the system due to competition of AFM and FM interactions resulting in some finite size spin clusters formation which generates the glassy state [266, 267]. Furthermore, similar magnetization behavior has been observed in partially disordered La_2NiMnO_6 [268]

and has been explained on the basis of two FM phases. However, Fig. 5.2 (XAS), shows the presence of only Co^{3+}-Fe^{3+} ions in LPCFO. Thus, DC magnetization data of LPCFO, combined with XAS results, clearly suggests a single magnetic phase in this material. Therefore, observed two magnetic features in the present work are the intrinsic parts of a homogeneous system in the presence of anti-site defects.

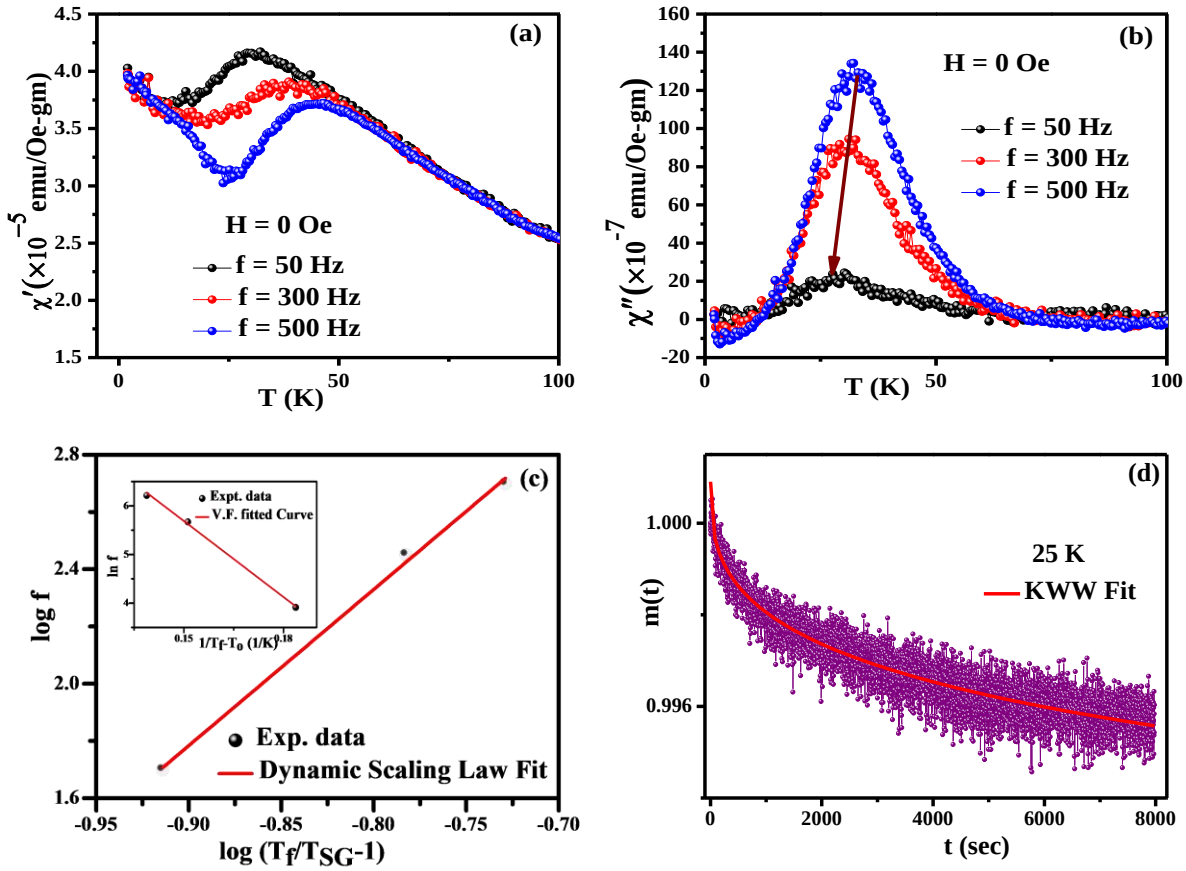

Figure 5.4: The temperature dependent real χ' (T) **(a)** and imaginary χ'' (T) **(b)** part of AC susceptibility of LPCFO at zero field. **(c)** Dynamic Scaling fit of log *f* Vs log (T_f/T_{SG} -1). **Inset** : Vogel-Fulcher fit of ln *f* Vs 1/(T_f-T_o) curve. **(d)**: TRM data at 25 K fitted with KWW equation.

Further, to confirm the nature of the glassy state (spin glass or cluster glass) in LPCFO, Mydosh parameter was calculated using the equation [269]

$$p = \frac{\Delta T_f}{T_f \Delta log_{10}(f)} \tag{5.2}$$

where, T_f is freezing temperature at frequency *f*, $\Delta T_f = T_{f1} - T_{f2}$. The obtained value of p for LPCFO system is ~ 0.095 which lies in the cluster glass regime. The freezing phenomenon can also be studied by the dynamic scaling law [124, 126],

$$f = f_0 \left(\frac{T_f - T_{SG}}{T_{SG}}\right)^{z\nu} \tag{5.3}$$

where, T_{SG} is spin glass freezing temperature, τ_0 is spin flipping time $(\tau_0) = \frac{1}{f_o}$ and z*ν* is the dynamical critical exponent. We have fitted data with equation (5.3) as shown in fig. 5.4c. The obtained related parameters are $\tau_0 = 5.988\times10^{-7} \pm 10^{-7}$ s, T_{SG} = 27.49 ± 0.68 K and z*ν* = 4.59± 0.68. The value of z*ν* lies between 4 to12 indicating the glassy state. Indeed, for a canonical SG state, value of τ_0 lies typically between ~ 10^{-12} - 10^{-13} s. However, the τ_0 value obtained from this fit is very large, indicating the freezing of magnetic clusters rather than individual spins [124, 126]. The presence of reentrant cluster glass (RCG) at low temperature is also verified with Vogel-Fulcher (VF) law [129]:

$$f = f_0 \exp\left(-\frac{E_A}{K_B(T_f - T_0)}\right) \tag{5.4}$$

where, T_o is VF temperature and E_A is activation energy. Eventually, VF law gives the information about inter-cluster interaction and T_o is also known as inter-cluster interaction strength. The VF fitted plot is shown in inset of fig.5.4c. The yielded parameters from the fit are $f_0 \sim 10^6$ Hz or $\tau_0 \sim 10^{-7}$ s, T_0 = 25.02 ± 0.79 K and E_A/K_B = 39.4 ± 3.00 K. The larger value of τ_0 again ruled out the presence of SG state and confirms the presence of CG state at low temperature. Further we have analyzed the data by Kohlrausch Williams Watt (KWW) [125] experimental eq. which is given by

$$m(t) = m_0 - m_g exp\left\{-\left(\frac{t}{\tau}\right)^{\beta}\right\} \quad (5.5)$$

where, m_o is initial remanent magnetization, m_g is magnetization of glass component, β is the stretching exponent and τ is the characteristic relaxation time constant. This method is well known for identification of glassy systems and value of β lies in between 0 and 1 for the glassy systems. The time dependent thermo-remanent magnetization (TRM) m(t) was measured below the freezing temperature T_f with a cooling field of 100 Oe. This TRM data were employed by KWW eq. and shown in fig. 5.4d. The obtained value of β from KWW fit is 0.248±0.04, which further confirms the existence of cluster glass state. Hence, the present DP LPCFO system shows reentrant cluster glass (RCG) at low temperature.

5.3.4 Dielectric Study:

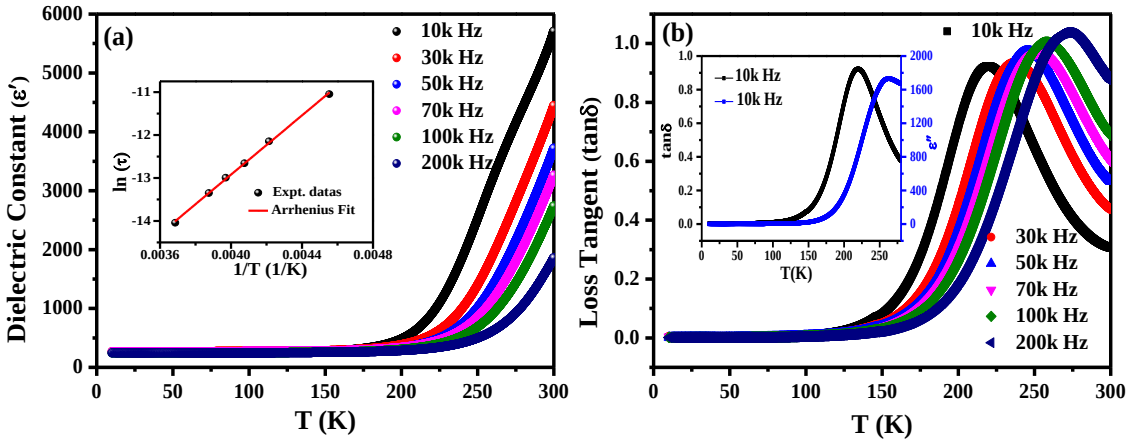

Figure 5.5: **(a)** Temperature dependent dielectric constant (ϵ') of LPCFO. **Inset:** Arrhenius fit of dielectric relaxation of LPCFO. **(b)** Temperature dependent dielectric tangent loss ($tan\delta$) of LPCFO. **Inset:** a comparative plot of $tan\delta$(T) and imaginary part of dielectric function ϵ"(T) at 10 kHz frequency.

Fig. 5.5a and 5.5b show the temperature dependent dielectric constant (ϵ') and loss tangent (tanδ) of LPCFO material at different frequencies. LPCFO exhibits huge dielectric constant (~6000) and low loss tangent (~1.1) at room temperature (RT). Such larger value of

ϵ' and low value of tanδ at RT are very advantageous for applications in capacitor, transducer and microwave [270, 271]. From fig. 5.5a, it can be seen that upto 150 K, ϵ' value is very small (~300) and independent of applied frequency and temperature indicating the observed dielectric behavior is intrinsic. Further, on moving from 150 K to higher temperature, ϵ' and tanδ abruptly increases with temperature and shows strong frequency dependence. One possible reason for the sudden change in ϵ' and tanδ values might be the space charge polarization and extrinsic factors [272]. However, there is no existence of permanent electric dipole in the present system as neither $tan\delta$ (T) nor ϵ" (T) merge together (inset of fig. 5.5b) [273]. From fig. 5.5b, it is also clear that tanδ peak shifts towards high temperature with increase of frequency. Thus, this dielectric relaxation in LPCFO is thermally activated relaxation process. Presence of accumulated charge carriers in different regions of system causes the dielectric relaxation which is known as Maxwell-Wagner (MW) relaxation. Hence, strong frequency dependence, large ϵ' and abrupt change in tanδ at (T≥150 K) indicates the relaxation process to be due to extrinsic polarization or MW effect [274]. Being thermally activated, relaxation phenomenon should follow Arrhenius law:

$$\tau = \tau_0 \exp(\frac{E_A}{K_B T}) \quad (5.6)$$

where, τ is relaxation time, τ_0 is pre-exponential factor and E_A is activation energy for the relaxation phenomenon. The plot between lnτ and 1/T is shown in inset of fig. 5.5a. The calculated value of τ_0 and E_A from the Arrhenius fit is 10^{-12} sec and 0.297 eV respectively.

5.3.5 Resistivity Study:

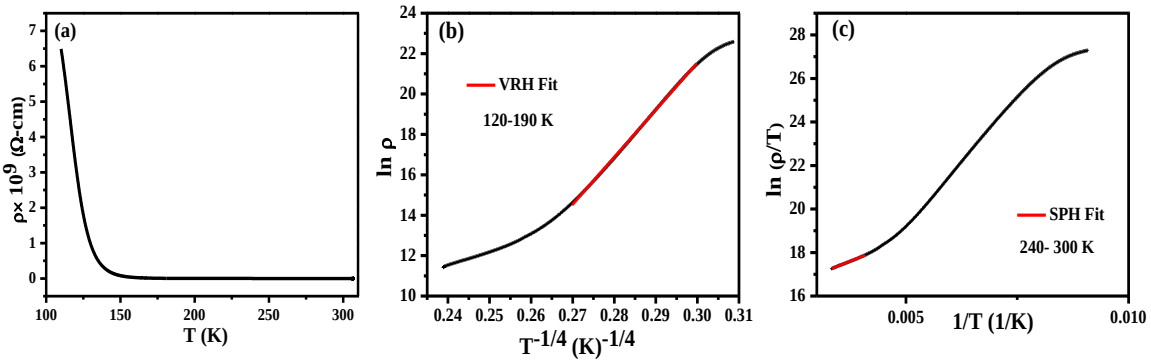

Figure 5.6: **(a)** Temperature dependent resistivity ρ(T) curve of LPCFO at zero magnetic field. **(b)** 3-d VRH fit of ρ(T) at 120 – 190 K temperature range. **(c)** SPH fit of ρ(T) at 240 – 300 K temperature range.

We have also measured the resistivity as a function of temperature. Fig. 5.6a depicts the temperature dependent dc resistivity ρ(T) of LPCFO. A semiconducting like behaviour is exhibited by LPCFO compound in 110-300 K temperature range. The high value of electrical resistivity below 110 K is beyond the limit of our measurement setup. We have fitted the electrical resistivity data of LPCFO by Mott's 3-dimensional variable range hopping (VRH), $\rho = \rho_o \exp(T_o/T)^{1/4}$ [where ρ_o is exponential factor and T_o is characteristic Mott temperature] [275]. The low temperature (120-190 K) data is well fitted by 3-d VRH model which is shown in fig. 5.6b. The obtained value of T_o from VRH fitting is 2.84×10^9 K. On the other hand, the high temperature resistivity data fitted by small polaron hopping (SPH) model [fig. 5.6c], $\rho = \rho_o T \exp(E_a/k_B T)$ [where E_a is activation energy and k_B is Boltzmann constant] [276]. The obtained activation energy from SPH fitting is 0.0698 eV.

5.3.6 Magneto-dielectric Study:

Further, to observe the effect of magnetic field on dielectric constant, we have carried out the magnetic field dependent dielectric constant measurement. Fig. 5.7a shows the percentage magneto-dielectricity (MD%) of LPCFO at 10 kHz frequency for different

temperatures. The MD% can be calculated as MD % = $\frac{\epsilon(\mathrm{H})-\epsilon(0)}{\epsilon(0)} \times 100\%$, where, $\epsilon(\mathrm{H})$ and $\epsilon(0)$ correspond to value of dielectric constant at magnetic field H and value of dielectric constant at zero magnetic field respectively. Inset of fig. 5.7a shows the pictorial diagram of MD% with temperature at 1.3 T magnetic field. LPCFO shows MD behaviour in two different regions, at low temperature region (25-80 K) and at high temperature region (125- 275 K). A small negative MD is observed for low temperature region (25-80 K) with maximum (-0.42%) at 50 K. At high temperature region (125-275 K), maximum ~ -4% MD is found at 200 K. The observation of such MDE in particular LPCFO is astonishing as no MDE has been reported in both parent compounds (LCFO and PCFO). In literature, the contribution of some major factors have been suggested in magneto-dielectric effect, including magneto–resistance (MR) [277], magneto-striction [278], spin pair correlation [279], spin lattice coupling [280, 281], electromagnon scattering [282], polaron mechanism [283], and dipole relaxation [284]. In the present case, the negative MD at low temperature (LT) can be explained by presence of reentrant cluster glass in this material. It has been discussed earlier that RCG behaviour in LPCFO is due to competing magnetic exchange interactions which are induced by antisite disorder. Therefore, presence of negative MD at LT shows a correlation between spin orientations on the Co and Fe sub lattices. Hence, at low temperature (25-80 K), magnetically frustrated or distorted magnetic phenomenon might be the cause of observed MDE in LPCFO indicating the coupling between spin and dipole moment. MDE has also been observed in SG or RCG states in La_2CoIrO_6 [255], $LaFe_{0.5}Mn_{0.5}O_3$ [256], Sm_2NiMnO_6 [103]. But in partially disordered La_2NiMnO_6 in the SG state, no MDE was observed and has been explained by the suppression of hopping contribution as well as it has been suggested the contribution to the

dielectric constant essentially from electron and phonon [20]. In the present investigation, though we could not measure the resistivity below 100 K because of our experimental limitation, even the existence of MDE suggest the presence of hopping mechanism as variable range hopping exists down to the lowest temperature of measurement (110K).

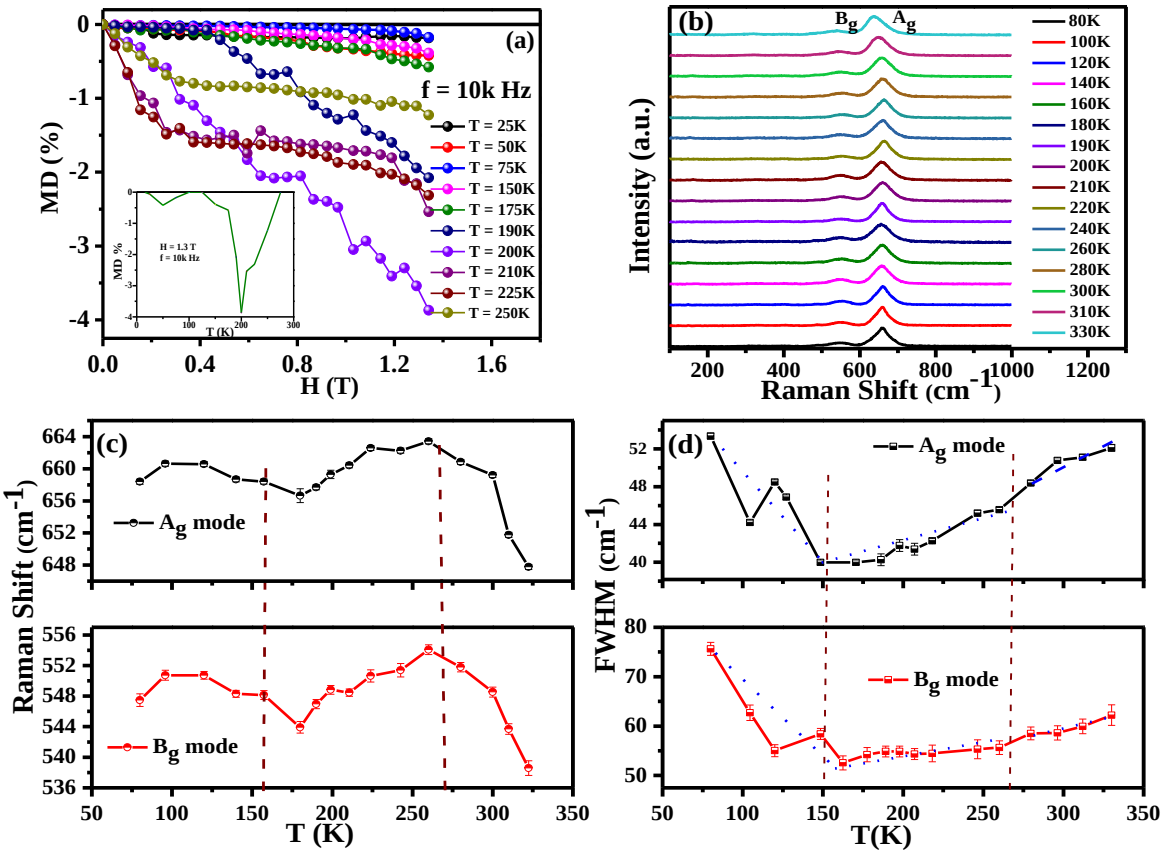

Figure 5.7(a): Magneto dielectric (%) as a function of magnetic field for LPCFO at different temperatures. **Inset:** Raw pictorial diagram of Magneto dielectric (%) Vs. temperature at 1.3 T magnetic field. **(b)** Raman scattering intensity of LPCFO at different temperatures (80-330 K) as a function of Raman shift. **(c**) Temperature dependence of the phonon positions of two typical modes (A_g and B_g) observed for LPCFO. Brown vertical dotted lines represent anomalies. **(d**) Temperature dependence of the Raman line widths (FWHM) of A_g and B_g modes. Blue dotted line shows the different slopes. Brown vertical dotted lines represent anomalies.

Origin of negative MD at high temperature range (125-275 K) can be explained by spin lattice interaction. As, this effect has been observed in LPCFO below the magnetic transition temperature (T_N) and the fact that LPCFO system is not a typical magneto-striction

material, therefore, the possibility of other factors like magneto-striction and MR can be ruled out as the origin of the observed MDE. In addition, MR effect is also absent in present system. Hence, to explain the MD behavior due to spin lattice correlation, we have analyzed the change in phonon structure. Figure 5.7b displays the experimental change in scattering intensity as a function of Raman shift at different temperatures (80-330 K). The Raman spectra of $La_{1.8}Pr_{0.2}CoFeO_6$ is similar to that of Tb_2NiMnO_6 [21] and Pr_2NiMnO_6 [99] which have same $P2_1/n$ symmetry. From group theory analysis, the total predicted vibration modes for perovskite can be expressed as $\Gamma = 12A_g+12\ B_g+18A_u+18\ B_u$. In this regard, there are 24 Raman active modes ($12A_g+12\ B_g$) and 33 Infrared (IR) active modes ($17A_u+16\ B_u$) and 3 acoustic modes ($A_u+2\ B_u$) [285, 286]. These Raman active modes appear due to symmetric and antisymmetric stretching of BO_6 octahedron. For present investigation, we have focused two Raman modes which are positioned at ~ 550 cm^{-1} and ~ 660 cm^{-1}. The first 550 cm^{-1} Raman mode (B_g mode) arises due to antisymmetric stretching of BO_6 octahedra, whereas, second Raman mode at 660 cm^{-1} (A_g mode) corresponds to symmetric stretching of octahedron [103, 287]. The temperature dependent phonon energy (Raman shift) and Full Width Half Maximum (FWHM) of both modes are displayed in fig. 5.7c and 5.7d. A clear anomaly (~270 K) below T_N can be seen from both the graphs in phonon frequencies for both modes suggesting the existence of spin-phonon coupling. Reduction of Raman shift with decrease in temperature indicates the softening behavior which is found in both modes down to ~150K. Similar trend or anomalies are visible in FWHM for both the modes. In insulating or semiconducting materials, Raman line widths are unaffected by a lattice volume change as these are considerably related to phonon lifetime. However, they are influenced by spin lattice coupling. Therefore, this hardening to softening transition in phonon modes with

decrease in temperature further suggests the presence of spin lattice coupling at high temperature region (125-275 K) [287]. However, above 275 K the MD disappears even though magnetic order persists above 275 K. Once again this result is not consistent with that La_2NiMnO_6 system [20] where this high temperature MD has been explained by the spin-spin correlation. Furthermore, the maximum MD appears at the temperature (~200 K) where the dipolar relaxation occurs. This implicates that MD follows the relaxation phenomenon [284]. Nevertheless, it has already been discussed above that asymmetric hopping mechanism (in the present case VRH) due to polaron formation mainly contributes to the dielectric relaxation [103]. Therefore, it can be suggested from the Raman effect measurement that the spin-lattice coupling which in effect induces the asymmetric hopping leads to contribute to the dielectric relaxation.

5.4 Conclusion:

Double perovskite $La_{1.8}Pr_{0.2}CoFeO_6$ sample was synthesized via solid state route. A single phase monoclinic crystal structure with $P2_1/n$ symmetry was confirmed by the XRD analysis. XAS technique identifies the +3 oxidation state of Co with low spin state and Fe ion with high spin state at room temperature. The magnetic analysis of LPCFO reflects that the system possesses canted antiferromagnetic nature above room temperature. Presence of reentrant cluster glass state is also confirmed by analyzing AC susceptibility at low temperature. Furthermore, LPCFO has high dielectric constant, low loss tangent and exhibits thermally activated relaxation mechanism. The magneto dielectric result indicates that LPCFO system has negative MD of ~0.42% and ~4% in low and high temperature region respectively. Moreover, temperature dependent Raman analysis demonstrates the spin lattice interaction which may be the origin of MDE in LPCFO. Therefore, the presence of high dielectric

constant, low loss tangent at room temperature along with MDE make this LPCFO material, a potential candidate for different applications such as in non volatile memories, faster data processing speeds with less power usages, large magnetic storage densities and magneto-dielectric sensors etc.